Ageing Effects on Exhaust Gas Catalysts: Microscopic Changes Captured by X-Ray Tomography

To cite this article: G Hofmann *et al* 2014 *J. Phys.: Conf. Ser.* **499** 012017

View the article online for updates and enhancements.

Related content

- The nanotomography endstation at the PETRA III Imaging Beamline
  M Ogurreck, F Wilde, J Herzen et al.

- Maia X-ray fluorescence imaging: Capturing detail in complex natural samples
  C G Ryan, D P Siddons, R Kirkham et al.

- New Energy Sources: in-situ Characterisation of Fuel Cell and Supercapacitor Components. Complementary Studies using Transmission, Fluorescence and Photoelectron Microscopy and Imaging
  B Bozzini, M Amati, A Gianoncelli et al.

Recent citations

- Fabian Wilde *et al*

- Modeling reaction-diffusion processes within catalyst washcoats: I. Microscale processes based on three-dimensional reconstructions
  Canan Karakaya *et al*

Ageing Effects on Exhaust Gas Catalysts: Microscopic Changes Captured by X-Ray Tomography

G Hofmann[1], A Rochet[1], S Baier[1], M Casapu[1], S Ritter[2], F Wilde[3], M Ogurreck[3], F Beckmann[3] and J-D Grunwaldt[1]

[1] Institute for Chemical Technology and Polymer Chemistry, Karlsruhe Institute of Technology, Karlsruhe, Germany

[2] Institute of Structural Physics, Technical University Dresden, Dresden, Germany

[3] Institute of Materials Research, Helmholtz-Zentrum Geesthacht, Geesthacht, Germany

E-mail: `grunwaldt@kit.edu`

Abstract. In this work we examine the different aspects of catalyst ageing with effects ranging from the nano to the macro scale. Underlining the general importance of combining different characterisation techniques, like transmission electron microscopy (TEM), X-ray absorption spectroscopy (XAS) and X-ray diffraction (XRD) for the nanoscale, we focus on the application of X-ray absorption micro-computed tomography (micro-CT) to capture macroscopic changes in the µm to mm scale. Two series of tomographic measurements were carried out: (i) investigation of three differently treated samples by collecting one channel from a fresh, a conditioned and an aged monolith and (ii) examination of one single coated honeycomb channel with 4 wt% Pt/γ-Al_2O_3 and for comparison one with pure γ-Al_2O_3 washcoat, which have been measured in a non-destructive ex situ manner at the same position after each ageing treatment.

Main observations of the tomographic study are: (1) coating inhomogeneities between different channels taken from the same honeycomb and between different honeycombs, (2) formation of cracks in the washcoat material and (3) formation of macroscopic Pt particles in the case of 4 wt% Pt/γ-Al_2O_3 washcoat. Particularly valuable is the non-destructive ex situ investigation after different ageing steps on the same channel using X-ray tomography.

1. Introduction

Exhaust gas catalysts are an inherent part in modern combustion vehicles which remove harmful components from the exhaust gas stream [1, 2, 3]. Emission limits being progressively restricted, the ideal aftertreatment system must show very high catalytic performance, i.e. full conversion of all harmful components, and a very long operation time. In spite of major achievements, the insufficient catalytic activity at low temperatures and the durability of exhaust gas aftertreatment systems are still major issues for the automotive industry. Common mechanisms of chemical or thermal deactivation comprise sintering of active sites, fouling or poisoning. These processes require characterisation across different length scales, ranging from the exhaust gas system over the monolithic structure down to the atomic scale [3, 4].

A synthetic ageing is usually applied to simulate the effects of ageing under real conditions in a shorter time frame and being less costly [5]. Hence, we tackle here in a first step the impact of the thermal ageing for a Pt-based model monolithic diesel oxidation catalyst (DOC) [6] on

different length scales. As DOC catalysts are three-dimensional objects in terms of their shape, composition, porosity and arrangement, it is reasonable to characterise them by a 3D-technique, such as X-ray tomography [7, 8].

In this paper the potential of X-ray micro-computed tomography (micro-CT) in capturing temperature induced structural and morphological changes on the micrometer scale [9, 10] is evaluated in combination with results obtained by more conventional methods such as bulk sensitive X-ray diffraction (XRD) and X-ray absorption spectroscopy (XAS) as well as transmission electron microscopy (TEM) which provide atomic scale information [11, 12]. This approach utilising X-ray absorption tomography is complementary to investigations with scanning electron microscopy (SEM), see e.g. refs. [1, 3], which beneficially allows, if combined with energy-dispersive X-ray spectroscopy (EDX), the determination of the elemental distribution in the washcoat [13]. Unfortunately, this latter technique eliminates possibilities for further studies of exactly the same sample due to its destructive sample preparation.

To demonstrate the strength of X-ray absorption tomography in this respect, two series of measurements were carried out: (i) the investigation of 4 wt% $Pt/\gamma\text{-Al}_2O_3$ coated honeycombs using three different samples by collecting one channel from a fresh, a conditioned and an aged monolith, shown in section 4.1, and (ii) using one single coated honeycomb channel from 4 wt% $Pt/\gamma\text{-Al}_2O_3$ and one from pure $\gamma\text{-Al}_2O_3$ for comparison, which have been measured at the same position after each treatment by conducting a non-destructive ex situ study as presented in section 4.2.

2. Sample Preparation, Ageing Treatments and Characterisation Methods

2.1. Sample Preparation

In a first step, cylindrical honeycomb pieces (d=20 mm, h=50 mm) were drilled out from a 400 channel per square inch cordierite monolith. The model catalyst samples, with a high surface area washcoat, were obtained by dip-coating these cylinders with 4 wt% $Pt/\gamma\text{-Al}_2O_3$, which was prepared as described in [14]. Additionally, a sample coated with pure $\gamma\text{-Al}_2O_3$ was used as reference in the ex situ study presented in section 4.2.

After drying the samples they were calcined in a static air furnace at 500 °C for 2 h, which resulted in a washcoat layer thickness of about 50 μm in average.
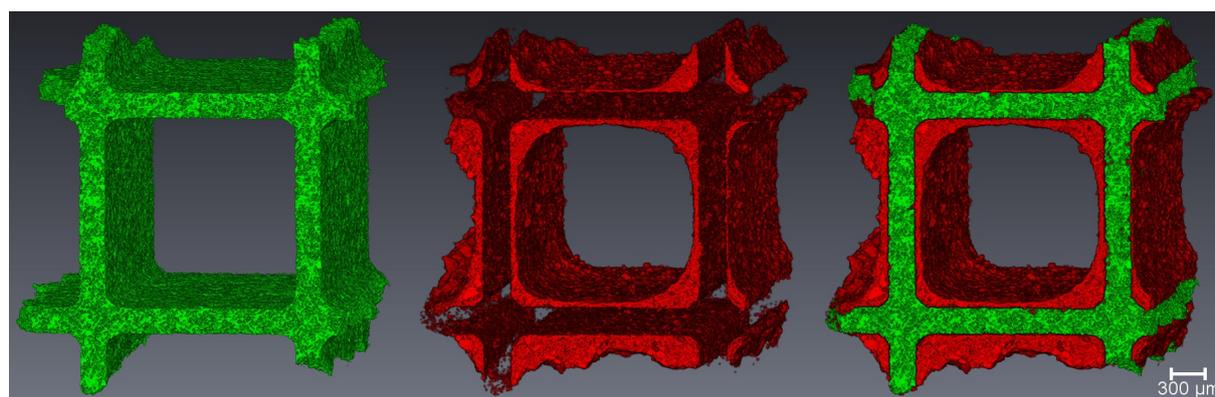

Figure 1. Volume rendering of a tomographic reconstruction showing a single coated honeycomb channel with dimensions $1.4 \times 1.4 \times 2.0\,\text{mm}^3$. Green: Cordierite, defining the structure of the honeycomb. Red: Washcoat, containing 4 wt% $Pt/\gamma\text{-Al}_2O_3$ as catalytic active material.

For tomographic investigations, a single channel was cut out from a honeycomb cylinder. Figure 1 shows an example for such a single channel in a tomographic reconstruction which

illustrates the two regions of the catalyst coated monolith: the cordierite defining the structure (green), and the washcoat layer (red).

2.2. Ageing Treatments

The study of 3 different channels from 3 different honeycombs, series (i), includes the following samples treated in a laboratory reactor: fresh samples corresponding to samples after the above mentioned calcination step, conditioned samples (denoted "cond.") treated for 4 h at 400 °C with 4% H_2/N_2, and hydrothermally aged samples (denoted "hyd. aged") heated for 10 h at 950 °C in 10% H_2O/air.

Ex situ tomography studies, series (ii), start with a fresh honeycomb channel coated with 4 wt% Pt/γ-Al_2O_3 and a channel with pure γ-Al_2O_3, respectively. The sequence of tomography measurements and thermal treatments in a static air furnace is schematically shown in Figure 2.

Fresh → Tomo. Scan → 600 °C 4 h → Tomo. Scan → 750 °C 4 h → Tomo. Scan → 950 °C 4 h → Tomo. Scan

Figure 2. Scheme for the sample treatment procedure during the ex situ X-ray absorption tomography study, series (ii), on a single channel: consecutive sample treatments in a static air furnace and tomography scans are performed.

This ageing procedure, from gentle influence at low temperatures to harsh conditions at highest temperatures, was chosen to benchmark the capabilities of X-ray tomography in detecting macroscopic changes in the sample. In this publication we only focus on the initial (fresh) and final state (ageing at 950 °C) to highlight the fundamental principle and to present first valuable results.

2.3. Characterisation Methods

The tomographic measurements presented in this study were performed at the "Imaging Beamline" P05 [15, 16] operated by the Helmholtz-Zentrum Geesthacht (HZG) at the synchrotron radiation source PETRA III (Deutsches Elektronen-Synchrotron, DESY, Hamburg). The undulator beamline is equipped with a Si(111) double crystal monochromator for energy filtering and a diffuser (rotating paper) to remove beam coherence. Accordingly, the sample is illuminated by a monochromatic, incoherent and parallel X-ray beam. The transmitted X-ray intensities through the sample are converted to visible light by a 300 µm thick $CdWO_4$ scintillator screen, which is magnified by an optical microscope and finally is recorded by a SciCam SC09000M CCD camera (EHD imaging). For further information on the used tomographic technique the reader is referred to a comprehensive review [17] and corresponding books [18, 19, 20] for fundamentals and principles.

X-ray absorption micro-tomography was used to measure the local absorption within the sample in three dimensions in a non-destructive way. Samples were scanned at a distance of 3-5 mm from the scintillator screen with an effective pixel size of 1.27 µm (10× magnification) and 0.2° steps over a 180° rotation at 16 keV. Reconstructions with a binning of 2 were obtained by a software maintained at P05 performing filtered back projection.

Additional analysis efforts were required for the samples measured in series (ii), since variations of sample position and orientation were encountered after remounting the samples into the sample stage after thermal treatments. This effect of "misaligned" samples is illustrated in Figure 3 (top). Therefore, before comparison and any further analysis, the corresponding data sets were "aligned" and transformed to a common 3D grid as depicted in Figure 3 (bottom). For

this purpose, the built-in image registration and resampling modules (utilising Lanczos filter) from Avizo Fire 8.0 by FEI VSG3D were used [21].
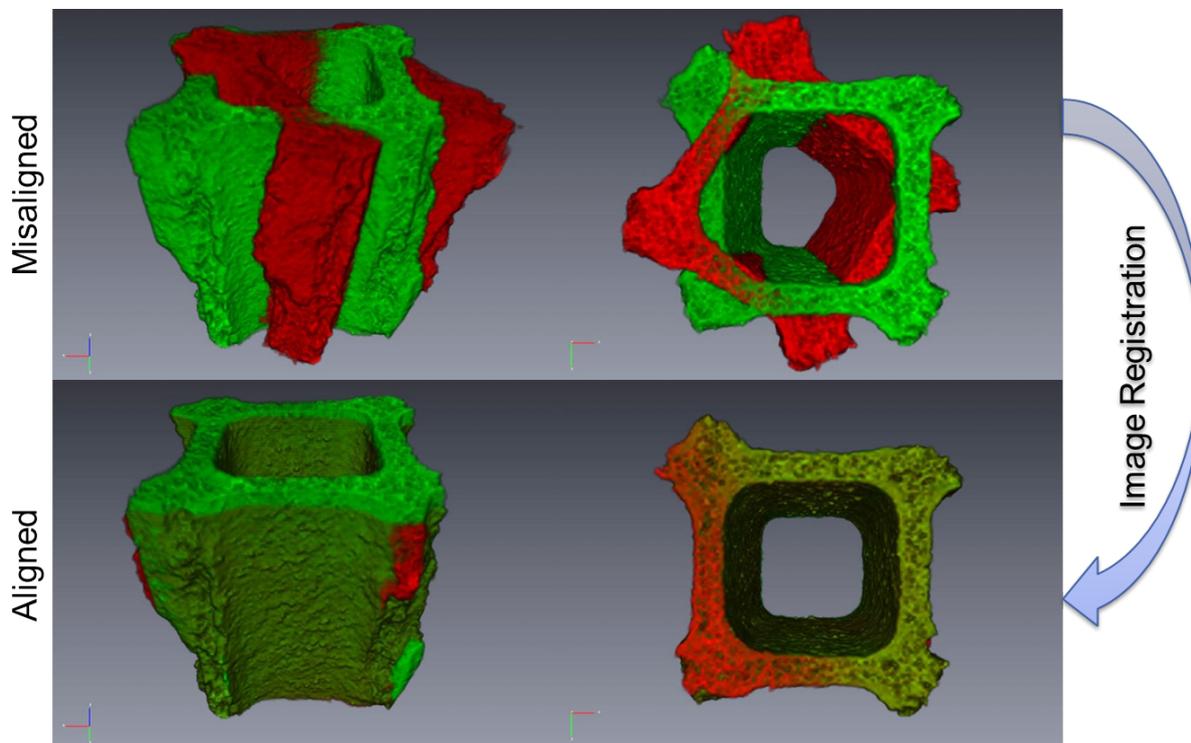

Figure 3. Consecutive sample remounting after ex situ heat treatments results in initially "misaligned" data sets shown in green and red (top). Image registration is used as the first step in data analysis to obtain "aligned" data sets (bottom).

To exclude modifications caused by sample handling, only the washcoat on walls inside a channel i.e. the red part inside the green walls in Figure 1, was considered and analysed for changes. Distinction of features between two data sets A and B is done by calculating their difference and raise it to the power of two, formally $(A - B)^2$.

For complementary analysis with more conventional techniques the sample material was collected by scratching off washcoat from fresh, conditioned or aged channels. XAS was measured on pelletised samples (diluted with cellulose) in transmission mode at the XAS beamline [22] at the ANKA synchrotron light source in Karlsruhe. The resulting spectra were energy calibrated by platinum foil as reference and normalised to pre- and post-edges using Athena from the Demeter software package [23].

TEM was carried out using a FEI Titan 80-300 aberration corrected microscope hosted at the Karlsruhe Nano Micro Facility (KNMF) at KIT. Samples were deposited on carbon coated Cu TEM grids. Data has been analysed using the Fiji software package [24].

X-ray powder diffraction patterns were obtained by using a Bruker D8 Advance X-ray diffractometer with a Cu anode operated at 35 kV and 45 mA. Data was background subtracted using the EVA software provided by Bruker and stacked by 1000 counts but kept unchanged in scaling for plotting.

3. Characterisation Results for Probing the Structure on a Nanoscale

The decrease of the catalytic activity during CO-oxidation and related reactions in exhaust gas catalysis due to thermal ageing is well known and has been previously reported in literature, e.g. [3, 14, 25]. For the Pt model catalyst used in this study the results of the XAS, TEM and XRD measurements are summarised in Figure 4.

The intensity and profile of the whiteline feature at the Pt L_3 edge (Figure 4a) reveal the presence of platinum oxide in the fresh catalyst, partial reduction of the conditioned sample and formation of metallic Pt after ageing (spectra superimposable to Pt foil reference spectra). The analysis of the EXAFS region (not shown) confirmed the formation of very large Pt particles after sintering at 950 °C.

This is in line with the TEM data (Figure 4b) which uncovered the presence of very small particles in the fresh catalyst (80% around 1.5 nm) and particle sizes of mainly 2 nm after conditioning. The particle size distribution changes significantly for the 950 °C aged catalyst, where only 40% of the particles remain below 2 nm and much larger sizes from 12 to 350 nm were found for 7% of the particles (not shown).

Using XRD we found some cordierite due to the above mentioned sample preparation. Together with Al_2O_3 it appears additionally to the labelled Pt pattern in the diffractograms (Figure 4c). The characteristic reflections stemming from metallic platinum are exclusively visible in the hydrothermally aged sample. This confirms the results obtained from TEM and XAS i.e. the formation of large and metallic Pt particles. All three characterisation techniques confirm the occurrence of a sintering process during ageing at high temperature that is observable on the nanoscale. However, changes in the system on the micrometer scale remain hidden to the above applied methods.
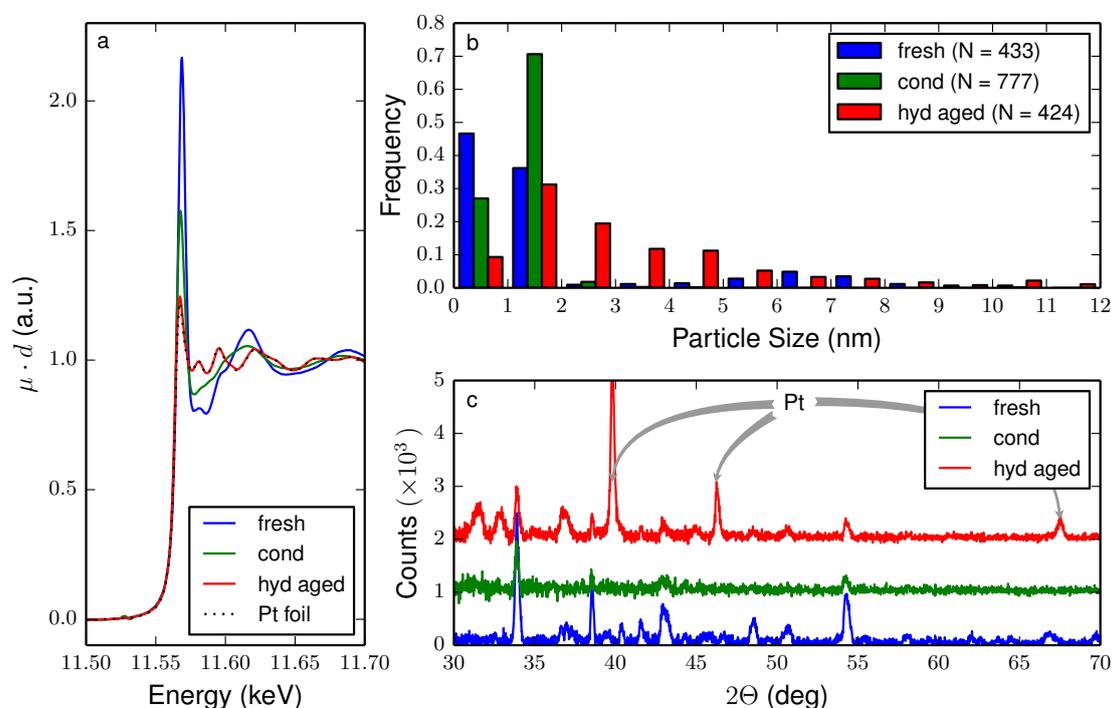

Figure 4. Characterisation results for the fresh, conditioned, and hydrothermally aged samples. **a)** XANES spectra showing the Pt L_3 edge of the samples and Pt foil as reference. **b)** Resulting particle size distribution from TEM by analysing a number of N Pt particles. **c)** Corresponding X-ray diffractograms.

4. Tomography Results

4.1. Monitoring of 3 Different Laboratory Prepared Channels

For the first series of measurements, series (i), three different channels were cut out from the corresponding fresh, conditioned and hydrothermally aged monoliths containing a 4 wt% Pt/γ-Al$_2$O$_3$ washcoat. Figure 5 presents for each sample a tomographically reconstructed slice perpendicular to the longitudinal channel axis. It can be observed that the cordierite has a very high porosity, which is maintained for all treatment steps, since it has been annealed at very high temperatures during fabrication.
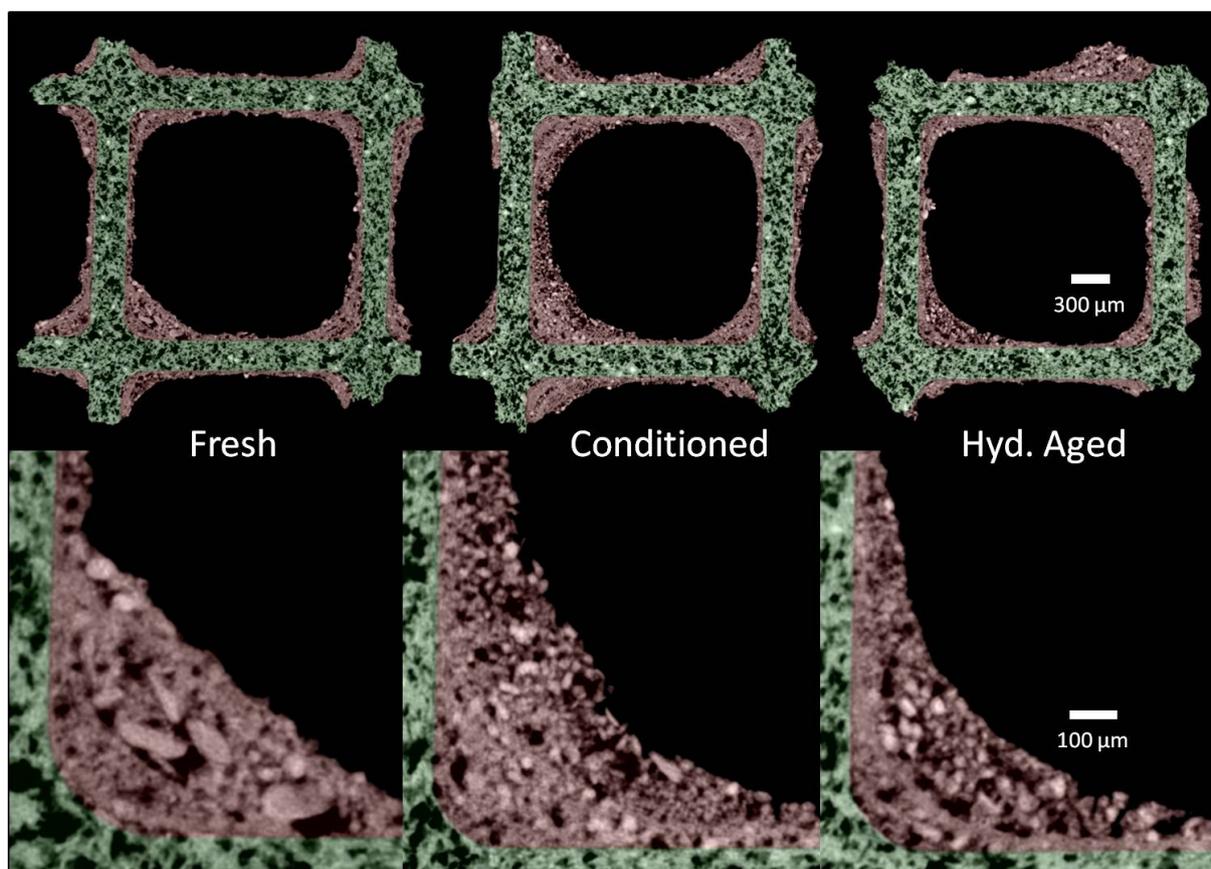

Figure 5. Three different honeycomb channels in fresh, conditioned and hydrothermally aged state. Top row: virtual cut perpendicular to the longitudinal channel axis showing the complete $1.4 \times 1.4 \, \text{mm}^2$ channel. Bottom row: magnification of the lower left corner. Green: Cordierite, defining the structure of the honeycomb. Red: Washcoat, containing 4 wt% Pt/γ-Al$_2$O$_3$. Black: void. Higher brightness corresponds to higher absorption.

Concerning the washcoat depicted in Figure 5, variation of the coating thickness and distribution is observed within and among the channels. This mainly originates from the dip-coating process during sample preparation and illustrates the limitation in obtaining a very homogeneous catalyst layer with the rather simple preparation method used here. This has effects on the utilisation of the catalyst material in the sample [26] and especially complicates comparison between samples. Moreover, the presence of smaller and brighter grains was observed, especially in the hydrothermally aged sample. As higher brightness corresponds to higher X-ray absorption, this could potentially be caused by sintering of the alumina carrier or, more likely, by Pt particles. Nevertheless, since different channels are scanned, it is difficult

to draw a clear conclusion on the origin of the mentioned features, except if a large number of samples would be investigated to obtain sufficient statistics. This emphasizes the need to study single channels in sequence at the same position as presented in the next section.

4.2. Ex situ Tomography Monitoring a Single Channel

To capture effects of thermal treatments on the sample, we need to investigate exactly the same sample before and after each treatment as evident from the above study. Therefore we use one single coated honeycomb channel with pure γ-Al$_2$O$_3$ and one with 4 wt% Pt/γ-Al$_2$O$_3$ washcoat. Thermal treatments and measurements of the samples are performed as schematically shown in Figure 2. On the obtained data we applied the above mentioned image registration as illustrated in Figure 3.

Here we compare the state of the fresh and the 4 h at 950 °C aged sample (cf. experimental part) for both mentioned samples. To exclude accidental modifications, as mentioned above, we only analyse the washcoat inside the channel. Therefore we apply a virtual clipping to the data as shown in Figure 6, to obtain relevant parts of the sample and a free view on a single wall.
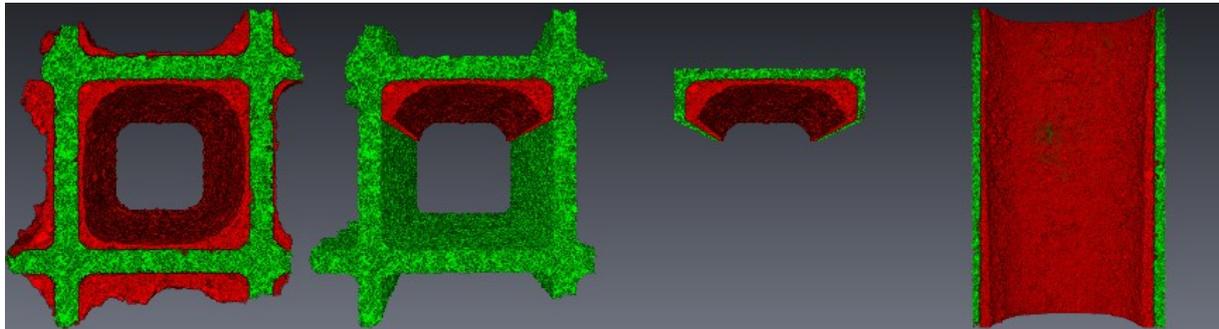

Figure 6. Illustration of virtual data clipping as used in the following discussion. To exclude accidental sample modifications, only the washcoat (red) inside the channel (green) is considered during evaluation. We apply virtual clipping to obtain a free view on the region of interest.

4.2.1. Ageing of γ-Al$_2$O$_3$ coated Channel - Evidence for Crack Formation

For the pure γ-Al$_2$O$_3$ coated reference sample after ageing treatments, we observed very strong formation of cracks and changes in the coating morphology along the channel, which originates from material displacement (Figure 7).

Crack formation already starts at temperatures as low as 600 °C and increases as a function of temperature. Thus, most distinct effects are obtained for ageing at 950 °C, as shown in Figure 7. Most of the differences (marked in red in Figure 7) between the fresh and aged samples are positioned in the vicinity of the cracks and no indication of distinct particle formation (higher density) on the plane area was found. These first observations underline that the morphological changes within the washcoat can be followed by X-ray absorption micro-tomography. This demonstrates the potential of the technique vividly.
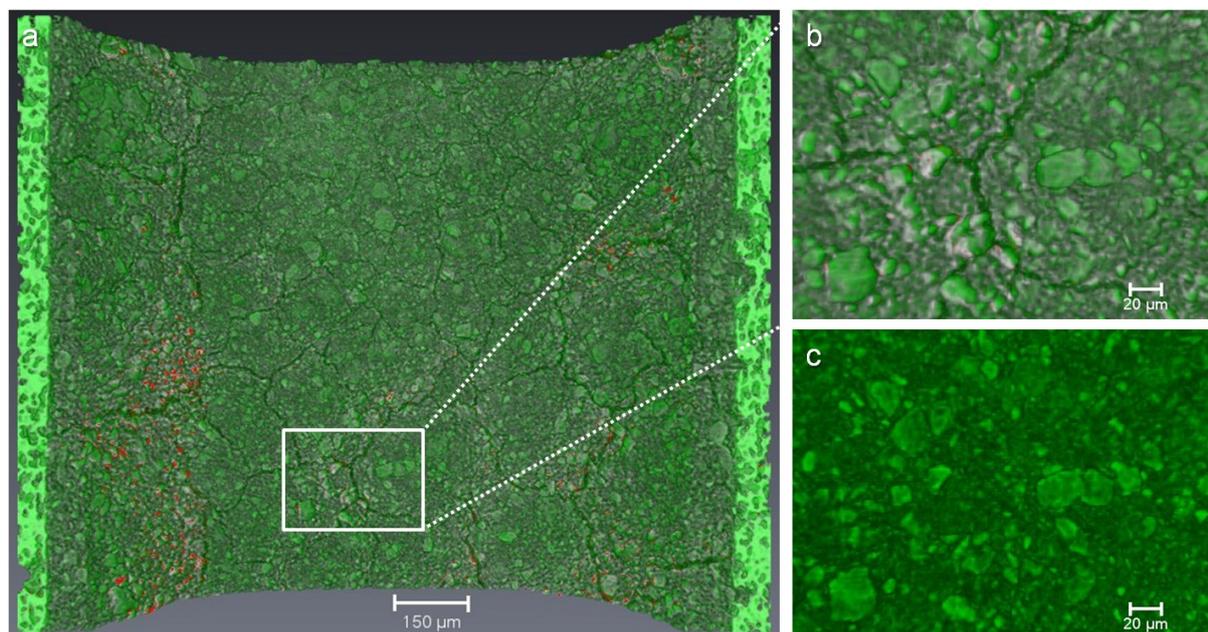
Figure 7. Direct overlay of initial (fresh, green) and final (ageing at $950\,°C$, gray) state for the pure γ-Al_2O_3 coated sample, where large differences are coloured in red. **a)** View on a wall viewed from inside the channel by applying a virtual clipping to the volume rendering parallel to the wall. Field of view $1.4 \times 1.1\,mm^2$. **b)** Zoom to region with formation of cracks. The extent and direction of material displacement due to the formation of the cracks can be followed by grains partially rendered in green (initial) and white (final) indicating the movement. **c)** For comparison the same area of the fresh sample without any crack.

4.2.2. Ageing of 4 wt% Pt/γ-Al_2O_3 coated Channel - Evidence for Particle Formation
In contrast to the pure alumina washcoat, the Pt containing sample shows crack formation to a much lesser extent (Figure 8). The location of the cracks is mostly at the corners of the channel where the layer thickness is biggest, as observed in Figure 5. In addition, numerous pronounced differences (marked in red in Figure 8) emerge due to the formation of larger particles. These regions with significantly higher amount of Pt are reliably detected by increased absorption as compared to the fresh sample. The results in Figure 8 show that their evolution is clearly not related to the crack formation as observed for the γ-Al_2O_3 channel. However, particle formation is not homogeneous across the sample, which may be due to variations in the Pt dispersion and distribution within the washcoat. The Pt-rich particles are already detected at $750\,°C$ (not shown here) and grow further in size and number as temperature increases up to $950\,°C$ in accordance to literature. These results are in line with the sintering behaviour uncovered by the XAS, TEM and XRD data but moreover these variations observed by micro X-ray absorption tomography show that thermal deterioration can also be observed on a macroscale, predicting a strong decrease in catalyst efficiency.

4.3. Comparison of results from series (i) and series (ii)
Comparing series (i) and series (ii) we first need to emphasize the methodical difference in conducting the experiments. In series (i) several different samples with diverse treatments were investigated. Differences in the washcoat amount and position can be seen immediately, as well as grains forming the washcoat and indications of sintered Pt particles. Statements on washcoat grains, their origin or evolution can hardly be made and there is a risk of misinterpretation,
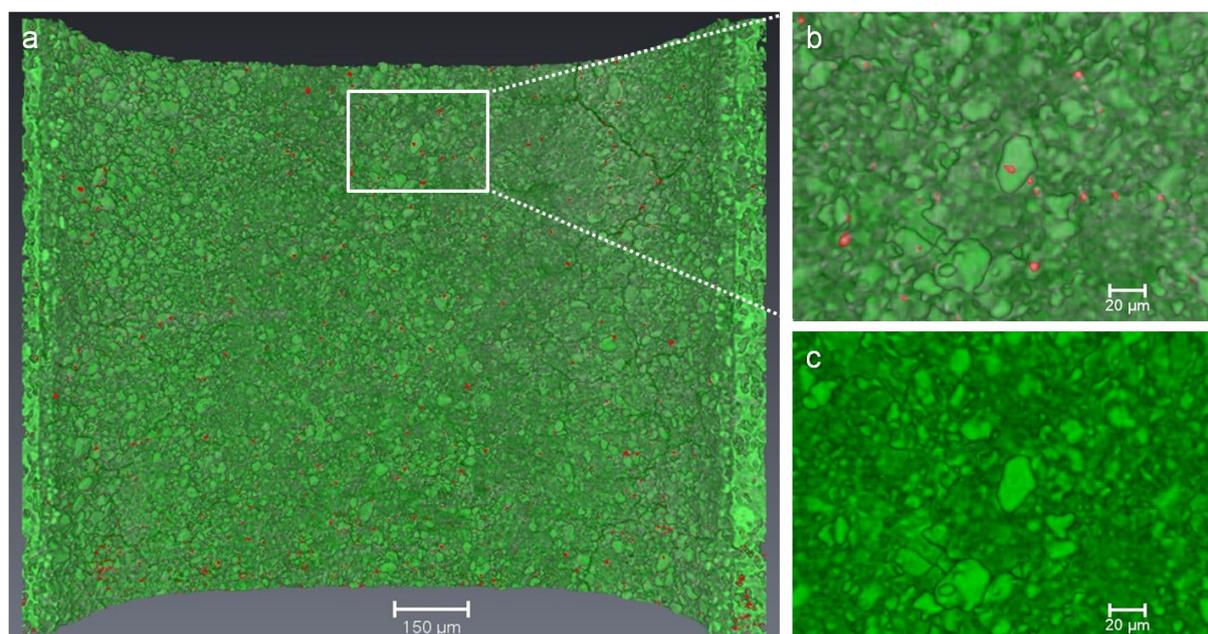
Figure 8. Direct overlay of initial (fresh, green) and final (ageing at 950 °C, gray) state for the Pt containing sample, where large differences are coloured in red. **a)** View on a wall viewed from inside the channel by applying a virtual clipping to the volume rendering parallel to the wall. Field of view $1.4 \times 1.1 \, \text{mm}^2$. **b)** Zoom to a region with particle formation. The position of the micrometer sized grains of the initial substrate remains unchanged in contrast to the uncoated sample. Newly formed particles are marked in red. **c)** For comparison the same area of the fresh sample.

since the initial state is unknown. Nevertheless it can be useful if these properties, like amount and distribution, have to be investigated.

Experiments in series (ii) are performed on exactly the same channel, which is subject to consecutive thermal treatments, to address the shortcoming of series (i). Consequently it allows to deduce statements of feature origin and evolution in the washcoat. On the other hand, no comparison to multiple other channels is done and has to be considered.

Both series provide equivalent information on the washcoat amount and distribution. In addition, series (ii) allows to reliably pinpoint sintered Pt particles and follow material movements as a function of the applied treatment.

The present study shows that such studies should be promoted in future where micro-tomography in X-ray absorption [7, 27], fluorescence [28, 29] or diffraction [30, 31] contrast is used on the same sample after different treatments or preferentially even in situ and thereby in short time intervals as reported in ref. [30].

5. Conclusions

This study of a model exhaust gas catalyst containing a 4 wt% $\text{Pt}/\gamma\text{-Al}_2\text{O}_3$ washcoat subjected to thermal ageing has demonstrated ageing effects both on the nano- and macroscale leading to catalyst deactivation. We have confirmed by XAS, TEM and XRD that, in accordance with literature, ageing alters properties on the nanometer scale like increasing the noble metal particle size distribution. Effects on the macroscale have been captured by non-destructive X-ray absorption micro-tomography of single honeycomb channels. Here monitoring of the same channel is of paramount importance to draw reliable conclusions.

Finally our present study revealed:

(i) Large variation of the amount and distribution of deposited washcoat on the channels, which is attributed to sample preparation. This affects the accessibility of catalyst material in the sample, controlled by mass transport, and especially complicates comparison between samples.

(ii) The formation of cracks in the washcoat material, leading to decrease in efficiency and in the worst case to rapid loss of material in the channel.

(iii) Particle sintering and appearance of micrometer sized particles in the 4 wt% Pt/γ-Al_2O_3 washcoat at $950\,°C$. This implies a rapid decrease in the number of small particles and thus potentially loss of highly active catalytic sites.

(iv) Spatially non-uniform formation of particles across the sample, which may be due to variations in the Pt dispersion and distribution within the washcoat.

These findings can be used in general to improve catalyst design and preparation. By applying advanced preparation methods, one can achieve more uniform and reproducible coating results for optimised catalyst utilisation. Enhanced stability and durability can be gained by introducing supports which are less prone to sintering and crack formation in conjunction with refined platinum dispersion in the coating suspension. Moreover, tomography can be used for characterisation of multi-layer catalysts to improve performance and to give input and feedback to the "product design" process to obtain long lasting and highly active catalysts.

In situ X-ray tomography with such samples under reactive conditions (gas flow, temperature) is highly desirable and is in principle possible due to the high penetrating nature of hard X-rays although dedicated in situ reactors still have to be developed. Besides the determination of the local absorption, different characteristics of the sample can be addressed by choosing appropriate tomographic contrasts. These are for example fluorescence for mapping the elemental distribution, diffraction for distinguishing crystalline phases or phase-contrast for investigating weakly absorbing samples. Altogether this renders the technique very versatile and capable of providing complementary information to other characterisation techniques, e.g. electron microscopy. Especially the combination of electron microscopy and X-ray microscopy seems to be an excellent tool despite some efforts must still be made to bridge the resolution gap for in situ tomographic imaging using hard X-rays with a spatial resolution of 20 to 500 nm.

References

[1] Votsmeier M, Kreuzer T, Gieshoff J and Lepperhoff G 2000 *Automobile Exhaust Control. Ullmann's Encyclopedia of Industrial Chemistry* (Wiley-VCH) pp 407–424 URL http://dx.doi.org/10.1002/14356007.a03_189.pub2

[2] Heck R M, Farrauto R J and Gulati S T 2009 *Catalytic air pollution control: Commercial technology* 3rd ed (Hoboken and N.J: John Wiley) ISBN 0470275030

[3] Deutschmann O and Grunwaldt J-D 2013 *Chemie Ingenieur Technik* **85** 595–617 URL http://dx.doi.org/10.1002/cite.201200188

[4] Bell A T 2003 *Science* **299** 1688–1691 URL http://dx.doi.org/10.1126/science.1083671

[5] Andersson J, Antonsson M, Eurenius L, Olsson E and Skoglundh M 2007 *Applied Catalysis B: Environmental* **72** 71–81 ISSN 09263373 URL http://dx.doi.org/10.1016/j.apcatb.2006.10.011

[6] Russell A and Epling W S 2011 *Catalysis Reviews* **53** 337–423 URL http://dx.doi.org/10.1080/01614940.2011.596429

[7] Grunwaldt J-D and Schroer C G 2010 *Chemical Society Reviews* **39** 4741–4753 URL http://dx.doi.org/10.1039/c0cs00036a

[8] Grunwaldt J-D, Wagner J B and Dunin-Borkowski R E 2013 *ChemCatChem* **5** 62–80 URL http://dx.doi.org/10.1002/cctc.201200356

[9] Gibson E K, Zandbergen M W, Jacques, Simon D M, Biao C, Cernik R J, O'Brien M G, Di Michiel M, Weckhuysen B M and Beale A M 2013 *ACS Catalysis* **3** 339–347 URL http://dx.doi.org/10.1021/cs300746a

[10] Beale A M, Jacques, Simon D M and Weckhuysen B M 2010 *Chemical Society Reviews* **39** 4656–4672 URL http://dx.doi.org/10.1039/C0CS00089B

[11] Niemantsverdriet J W 2007 *Spectroscopy in catalysis: An introduction* 3rd ed (Weinheim: Wiley-VCH) ISBN 9783527316519

[12] Grunwaldt J-D, Kimmerle B, Baiker A, Boye P, Schroer C G, Glatzel P, Borca C N and Beckmann F 2009 *Catalysis Today* **145** 267–278 URL http://dx.doi.org/10.1016/j.cattod.2008.11.002

[13] Winkler A, Ferri D and Aguirre M 2009 *Applied Catalysis B: Environmental* **93** 177–184 URL http://dx.doi.org/10.1016/j.apcatb.2009.09.027

[14] Boubnov A, Gänzler A, Conrad S, Casapu M and Grunwaldt J-D 2013 *Topics in Catalysis* **56** 333–338 URL http://dx.doi.org/10.1007/s11244-013-9976-6

[15] Haibel A, Beckmann F, Dose T, Herzen J, Ogurreck M, Müller M and Schreyer A 2010 *Powder Diffraction* **25** 161–164 URL http://dx.doi.org/10.1154/1.3428364

[16] Haibel A, Ogurreck M, Beckmann F, Dose T, Wilde F, Herzen J, Müller M, Schreyer A, Nazmov V, Simon M, Last A and Mohr J 2010 *Proc. of SPIE* (*Developments in X-Ray Tomography VII* vol 7804) p 78040B URL http://dx.doi.org/10.1117/12.860852

[17] Landis E N and Keane D T 2010 *Materials Characterization* **61** 1305–1316 URL http://dx.doi.org/10.1016/j.matchar.2010.09.012

[18] Avinash C Kak, Malcolm Slaney 2001 *Principles of Computerized Tomographic Imaging* (IEEE Press) ISBN 9780898714944 URL http://www.slaney.org/pct/

[19] Buzug T M 2008 *Computed tomography: From Photon Statistics to Modern Cone-Beam CT* (Berlin and Heidelberg: Springer) URL http://dx.doi.org/10.1007/978-3-540-39408-2

[20] Herman G T 2009 *Fundamentals of Computerized Tomography: Image Reconstruction from Projections* Advances in Pattern Recognition. (Springer London) URL http://dx.doi.org/10.1007/978-1-84628-723-7

[21] Avizo Fire 8 - 3D Analysis Software for Materials Science URL http://www.vsg3d.com/avizo/fire

[22] Grunwaldt J-D, Hannemann S, Göttlicher J, Mangold S, Denecke M A and Baiker A 2005 *Physica Scripta* **2005** 769 URL http://dx.doi.org/10.1238/Physica.Topical.115a00769

[23] Ravel B and Newville M 2005 *Journal of Synchrotron Radiation* **12** 537–541 URL http://dx.doi.org/10.1107/S0909049505012719

[24] Schindelin J, Arganda-Carreras I, Frise E, Kaynig V, Longair M, Pietzsch T, Preibisch S, Rueden C, Saalfeld S, Schmid B, Tinevez J Y, White D J, Hartenstein V, Eliceiri K, Tomancak P and Cardona A 2012 *Nature Methods* **9** 676–682 URL http://dx.doi.org/10.1038/nmeth.2019

[25] Wiebenga M H, Kim C H, Schmieg S J, Oh S H, Brown D B, Kim D H, Lee J H and Peden C H 2012 *Catalysis Today* **184** 197–204 URL http://dx.doi.org/10.1016/j.cattod.2011.11.014

[26] Roy S, K Heibel A, Liu W and Boger T 2004 *Chemical Engineering Science* **59** 957–966 ISSN 00092509 URL http://dx.doi.org/10.1016/j.ces.2003.12.001

[27] Schroer C G, Kuhlmann M, Gunzler T F, Lengeler B, Richwin M, Griesebock B, Lützenkirchen-Hecht D, Frahm R, Ziegler E, Mashayekhi A, Haeffner D R, Grunwaldt J-D and Baiker A 2003 *Applied Physics Letters* **82** 3360–3362 URL http://dx.doi.org/10.1063/1.1573352

[28] Samber B, Silversmit G, Evens R, Schamphelaere K, Janssen C, Masschaele B, Hoorebeke L, Balcaen L, Vanhaecke F, Falkenberg G and Vincze L 2008 *Analytical and Bioanalytical Chemistry* **390** 267–271 URL http://dx.doi.org/10.1007/s00216-007-1694-0

[29] Basile F, Benito P, Bugani S, Nolf W d, Fornasari G, Janssens K, Morselli L, Scavetta E, Tonelli D and Vaccari A 2010 *Advanced Functional Materials* **20** 4117–4126 URL http://dx.doi.org/10.1002/adfm.201001004

[30] Jacques, Simon D M, Di Michiel M, Beale A M, Sochi T, O'Brien M G, Espinosa-Alonso L, Weckhuysen B M and Barnes P 2011 *Angewandte Chemie International Edition* **50** 10148–10152 URL http://dx.doi.org/10.1002/anie.201104604

[31] Álvarez-Murga M, Bleuet P and Hodeau J L 2012 *Journal of Applied Crystallography* **45** 1109–1124 URL http://dx.doi.org/10.1107/S0021889812041039